



Ultra-low loading of copper modified $\text{TiO}_2/\text{CeO}_2$ catalysts for low-temperature selective catalytic reduction of NO by NH_3

Lulu Li^a, Lei Zhang^c, Kaili Ma^a, Weixin Zou^a, Yuan Cao^a, Yan Xiong^d, Changjin Tang^{a,**}, Lin Dong^{a,b,*}

^a Key Laboratory of Mesoscopic Chemistry of MOE, School of Chemistry and Chemical Engineering, Nanjing University, Nanjing 210093, PR China

^b Jiangsu Key Laboratory of Vehicle Emissions Control, Center of Modern Analysis, Nanjing University, Nanjing 210093, PR China

^c College of Environmental and Chemistry Engineering, Chongqing Three Gorges University, Chongqing 404100, PR China

^d College of Chemistry and Pharmaceutical Engineering, Nanyang Normal University, Nanyang 473061, PR China

ARTICLE INFO

Article history:

Received 9 October 2016

Received in revised form 9 February 2017

Accepted 11 February 2017

Available online 14 February 2017

Keywords:

Selective catalytic reduction

$\text{TiO}_2/\text{CeO}_2$

Copper doping

SO_2 durability

Reaction mechanism

ABSTRACT

A series of ultra-low content copper-modified $\text{TiO}_2/\text{CeO}_2$ catalysts were prepared by wet impregnation method and tested for selective catalytic reduction of NO by NH_3 . The catalyst with a Cu/Ce molar ratio of 0.005 showed the best low-temperature activity and excellent sulfur-poisoning resistance. It was worth noting that the very small amounts of copper addition can lead to three times the activity at low temperature. The prepared catalysts were characterized by XRD, BET, Raman, XPS, NH_3 -TPD and the results revealed that the introduction of copper increased the amount of surface adsorbed oxygen and Ce^{3+} species on the catalyst surface and generated more Brønsted acid sites. The redox and surface acidic properties were also improved by the addition of Cu. All these factors played important roles in enhancing NH_3 -SCR performance of $\text{TiO}_2\text{-CuO}/\text{CeO}_2$ catalysts. Furthermore, *in situ* DRIFT experiments demonstrated that Cu doping enhanced the adsorption capacity of NH_3 while the appearance of CuO weakened the adsorption ability of bridging nitrates, both the two factors synergistically facilitated the NH_3 -SCR reaction proceed smoothly via the Eley-Rideal pathway.

© 2017 Elsevier B.V. All rights reserved.

1. Introduction

Nitrogen oxides (NO_x), as one kind of harmful gases, give rise to a lot of environmental problems, such as acid rain, photochemical smog, ozone depletion, which threaten human health to a great extent [1–3]. Along with the pursuit towards better living environment and the gradual stringent environmental legislation, NO_x emission becomes a research hotspot in the field of environmental protection. The selective catalytic reduction of NO_x by NH_3 ($\text{NH}_3\text{-SCR}$) is a typical efficient de NO_x technique for the emission reduction of NO_x from coal-fired power plants [4–6]. The commercial catalysts for this process are $\text{V}_2\text{O}_5\text{-MoO}_3(\text{WO}_3)/\text{TiO}_2$ catalysts due to their high NO_x removal efficiency at 300–400 °C [7,8]. However, the drawbacks of vanadium-based catalysts are also obvious, including vanadium toxicity, narrow operation tem-

perature window and low N_2 selectivity in the high temperature range, which constrain their industrial application [9–11]. Thus, developing environmental friendly $\text{NH}_3\text{-SCR}$ catalysts with wide-temperature operation window is still a challenge and a number of studies have been performed to exploit new appropriate catalysts. During the investigations in this field, CeTi-based catalysts have been found to be a kind of effective SCR catalysts with excellent performance and environmentally-benign characteristic. Li and co-workers found that Ce-Ti mixed oxides exhibited superior NO conversion and N_2 selectivity at 175–450 °C and proposed the Ce-O-Ti short-range order species were the active sites in $\text{NH}_3\text{-SCR}$ reaction for the first time [12]. Afterwards, Gao et al. compared the differences between various preparation methods over $\text{CeO}_2/\text{TiO}_2$ catalysts and pointed out that the catalyst prepared by the single step sol-gel could show better SCR activity [13]. In our previous work, a novel $\text{TiO}_2/\text{CeO}_2$ catalyst was developed and exhibited better SO_2 resistance than conventional $\text{CeO}_2/\text{TiO}_2$ catalysts. We thought the reason for the good sulfur durability over $\text{TiO}_2/\text{CeO}_2$ was that the dispersed TiO_2 could prevent the formation of sulfate crystal phase, which blocked the active sites of Ce—O—Ti [14]. But in consideration of the low-temperature activity, the reported CeTi-based $\text{NH}_3\text{-SCR}$ catalysts were still not very satisfactory. Therefore,

* Corresponding author at: Key Laboratory of Mesoscopic Chemistry of MOE, School of Chemistry and Chemical Engineering, Nanjing University, Nanjing, 210093, PR China.

** Corresponding author.

E-mail addresses: tangcj@nju.edu.cn (C. Tang), donglin@nju.edu.cn (L. Dong).

many transition metal oxides involving Cu, Mn, Fe, and W were used to improve their catalytic performance [15–18]. He et al. reported Ce_{0.2}W_{0.2}TiO_x catalyst prepared by a facile homogeneous precipitation showed over 90% NO conversion from 275 to 450 °C under GHSV = 500,000 h⁻¹ [9]. Liu et al. demonstrated that modifying CeO₂-TiO₂ catalyst with Cu could facilitate the low temperature catalytic activity and they attributed the promoting effects to the dual redox cycles (Cu²⁺ + Ce³⁺ ⇌ Cu⁺ + Ce⁴⁺, Cu²⁺ + Ti³⁺ ⇌ Cu⁺ + Ti⁴⁺) [19]. Du et al. then found that the addition of copper could also result in high SO₂ resistance, which was ascribed to the sacrificial formation of CuSO₄, preserving Ce⁴⁺ active sites [16]. The above researches stated that Cu was a good additive to improve the low-temperature SCR activity and SO₂ durability of CeTi-based catalysts. There is further research suggesting that the dispersion state of copper species over copper-based catalysts have great influence on their catalytic performance [20,21]. Kwak et al. reported that isolated copper species was beneficial to enhance the N₂ selectivity and large CuO clusters led to the occurrence of NH₃-SCR side reaction to produce more NO_x over Cu/Al₂O₃ catalyst [22]. The identity of Cu species is believed to be related directly to its content over copper-contained catalyst. Therefore, it is reasonably supposed that the loading amount of copper species has remarkable influence on catalytic performance for Cu-containing SCR catalysts. However, no attention has yet been paid to the examination of catalytic activity versus Cu loading and identity over TiO₂-CuO/CeO₂ catalysts where the ceria is the dominant component. Inspired by the above results, we are committed to study the structure-activity relationships over minor copper modified TiO₂/CeO₂ catalyst under different copper loading amount (molar ratio of Cu/Ce ≤ 1%) and taking into account of the roles of different Cu species on catalytic performance. In this work, a series of TiO₂-CuO/CeO₂ catalysts prepared by an impregnation method containing an extremely low loading concentration of copper (molar ratio of Cu/Ce ≤ 0.01) were exploited for low-temperature NH₃-SCR catalysts. The influence of Cu loading on redox, physical-chemical and catalytic properties were studied. The catalysts were characterized by means of N₂-physisorption, XRD, Raman, H₂-TPR, EPR, XPS, and NH₃-TPD. Finally, the reaction mechanism was investigated by *in situ* DRIFTS technology.

2. Experimental

2.1. Catalyst preparation and activity test

The catalysts were prepared by a facile wet impregnation method using tetrabutyl titanate, cerium nitrate hexahydrate and cupric nitrate as precursors. All chemicals used were of analytical grade. The CeO₂ support was obtained by direct thermal decomposition at 500 °C for 5 h through cerium nitrate hexahydrate. First, a certain amount tetrabutyl titanate was dissolved in ethanol with stirring in ice water bath. Then, prescribed amount of Cu(NO₃)₂·3H₂O and ceria were added to the above solution. The mixed solutions were vigorously stirred for 2 h and evaporated to remove the water at 100 °C. The resulting materials were dried at 110 °C for 12 h and finally calcined at 450 °C in flowing air for 5 h. The catalysts were denoted as Ti1/CeO₂ and Ti1Cu_y/CeO₂, where y (y=0.001, 0.005, 0.01) represented the molar ratio of Cu: Ce, the ratio of Ti: Ce was fixed at 1:9. As a reference, the traditional V₂O₅-WO₃/TiO₂ catalyst with V₂O₅ (1 wt%) and WO₃ (9 wt%) loadings was prepared by impregnation method according to literature [23,24]. The ammonium metavanadate and ammoniumparatungstate was used as precursors and nano TiO₂ as the support, then was calcined at 450 °C and its BET-surface area was 59.8 m²/g. Finally, all the samples were crushed and sieved to 40–60 mesh for test.

The catalytic performances of these samples for the selective catalytic reduction of NO by NH₃ in the presence of excess oxygen were determined under steady state. The reaction condition was: 500 ppm NO, 500 ppm NH₃, 5% O₂, 100 ppm SO₂ (when used), 5% H₂O (when used), and N₂ in balance. The sample (200 mg, GHSV of ca. 45,000 h⁻¹) was fitted in a quartz tube and pretreated in a high purified N₂ stream at 200 °C for 1 h. The reactions were carried out at different temperatures and the concentrations of NO, NH₃, NO₂ and N₂O were measured at 150 °C by a Thermo Fisher IS10 FTIR spectrometer equipped with a 2 m path-length gas cell (250 ml volume). The NO conversion and N₂ selectivity were calculated from the following equations:

$$\text{No conversion}(\%) = \frac{[\text{NO}]_{\text{in}} - [\text{NO}]_{\text{out}}}{[\text{NO}]_{\text{in}}} \times 100$$

$$\text{N}_2 \text{ selectivity}(\%) = \frac{[\text{NO}_2]_{\text{in}} - [\text{NO}]_{\text{out}} + [\text{NH}_3]_{\text{in}} - [\text{NH}]_{\text{out}} - [\text{NO}_2]_{\text{in}} - 2[\text{N}_2\text{O}]_{\text{out}}}{[\text{NO}]_{\text{in}} - [\text{NO}]_{\text{out}} + [\text{NH}_3]_{\text{in}} - [\text{NH}]_{\text{out}}} \times 100$$

2.2. Catalyst characterization

A Philips X'pert Pro diffractometer with Ni-filtered Cu K α 1 radiation (0.15408 nm) was used to collect X-ray powder diffraction (XRD) patterns. The X-ray tube was operated at 40 kV and 40 mA. The average crystallite size was calculated by Scherrer equation. The specific surface areas of samples were measured by N₂ physisorption at -196 °C on a Micromeritics ASAP-2020 analyzer. Before each adsorption measurement, the samples were activated for 3 h at 300 °C. Raman spectra were collected at room temperature on a Spex 1877 D triplemate spectrograph with 2 cm⁻¹ resolution. A 532 nm DPSS diode-pump solid semiconductor laser was used as the excitation source with power output of ca. 5 mW. H₂-temperature programmed reduction (H₂-TPR) experiments were carried out in a quartz U-type reactor connected to a thermal conductivity detector (TCD) with Ar-H₂ mixture (7.0% of H₂ by volume, 70 ml min⁻¹) as the reductant. Prior to the reduction, the sample (50 mg) was pretreated in a high purified N₂ stream at 200 °C for 1 h. EPR measurements were performed on a Bruker EMX-10/12 spectrometer operating at X-band frequency ($v \approx 9.4$ GHz) and 100-kHz field modulation. The spectra of these catalysts were recorded at 77 K. X-ray photoelectron spectra (XPS) were performed on a PHI 5000 VersaProbe system, using monochromatic K α radiation (1486.6 eV) operating at an accelerating power of 15 kW. The sample charging effects were compensated by calibrating all binding energies (BE) with the adventitious C 1 s peak at 284.6 eV. NH₃-temperature programmed desorption (NH₃-TPD) experiments were carried out on a multifunction chemisorption analyzer with a quartz U-tube reactor, detected by a thermal conductivity detector (TCD). About 100 mg of the sample was pretreated by passage of high purified He (40 ml min⁻¹) at 450 °C for 1 h. After pretreatment, the sample was saturated with high purified NH₃ (40 ml min⁻¹) at 100 °C for 1 h and subsequently flushed with the flowing high purified He (40 ml min⁻¹) at the same temperature for 1 h to remove gaseous and weakly adsorbed NH₃, then the sample was heated to 600 °C at a rate of 10 °C/min in the flowing high purified He (40 ml min⁻¹). *In situ* diffuse reflectance infrared Fourier transform spectra (*in situ* DRIFTS) were collected at a spectral resolution of 4 cm⁻¹ (number of scans, 32) on a Nicolet 5700 FT-IR spectrometer equipped with a high-sensitive MCT detector cooled by liquid N₂. The sample was pretreated with a high purified N₂ stream at 375 °C for 1 h to eliminate the physical adsorption of water and other impurities and then cooled to the desired reaction temperature. A background spectrum was collected under a flowing N₂ atmosphere and was subtracted from the sample spectra. The reaction conditions as follows: 500 ppm NH₃, 500 ppm NO, 5 vol.% O₂, N₂ balance and 100 ml min⁻¹ flow rate.

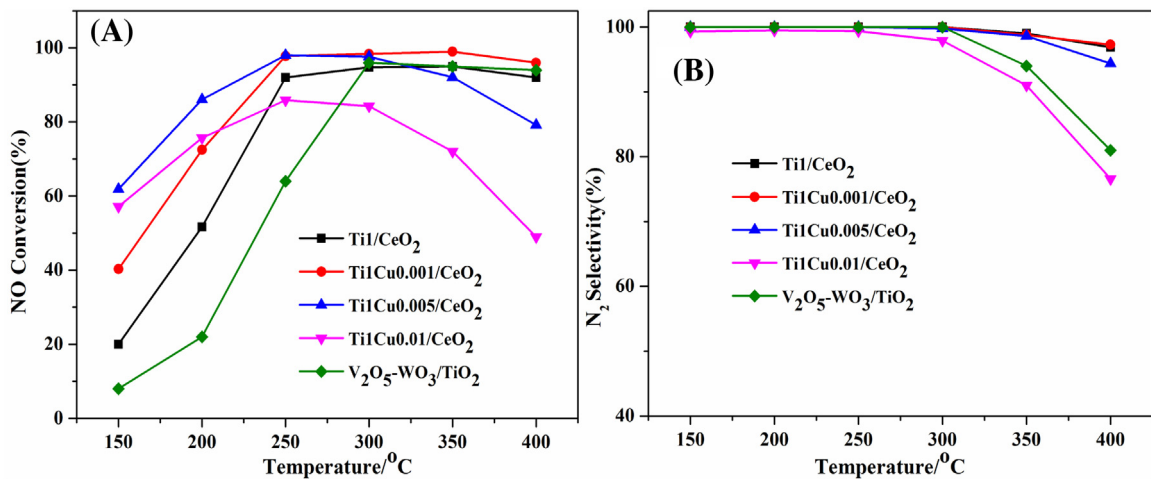


Fig. 1. The NO conversion and N₂ selectivity of the Ti1/CeO₂, Ti1Cu_y/CeO₂ and V₂O₅-WO₃/TiO₂ catalysts for NH₃-SCR reaction: (A) NO conversion (B) N₂ selectivity, Reaction conditions: 500 ppm NO, 500 ppm NH₃, 5 vol.% O₂, total flow rate 100 ml min⁻¹ and GHSV = 45,000 h⁻¹.

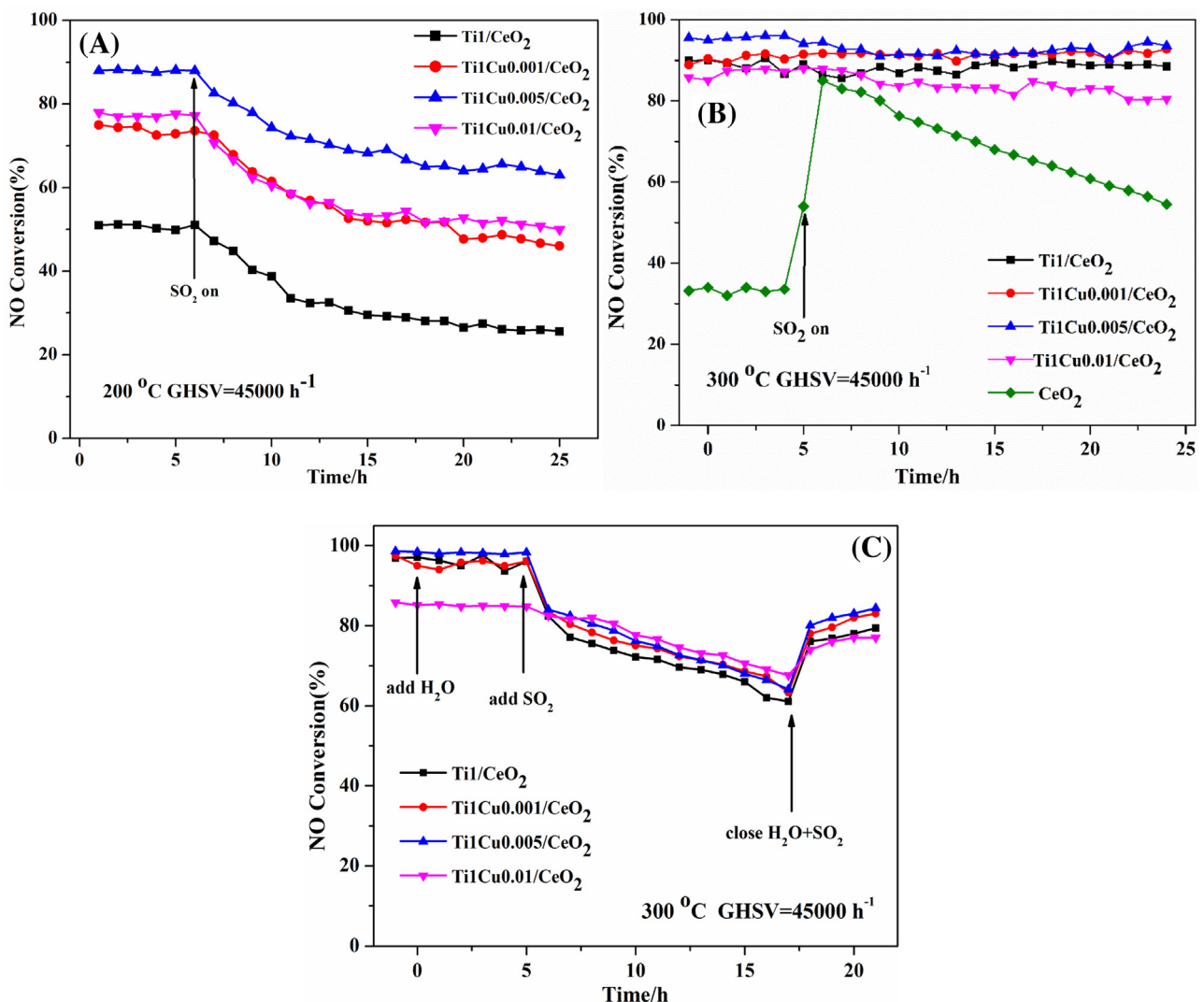


Fig. 2. The H₂O and SO₂ durability of these catalysts (A) SO₂ durability over Ti1/CeO₂ and Ti1Cu_y/CeO₂ catalysts at 200 °C (B) SO₂ durability over Ti1/CeO₂ and Ti1Cu_y/CeO₂ catalysts at 300 °C. (C) H₂O/H₂O + SO₂ durability over Ti1/CeO₂ and Ti1Cu_y/CeO₂ at 300 °C. Reaction conditions: 500 ppm NO, 500 ppm NH₃, 5 vol.% O₂, 200 ppm SO₂ (when used), 5 vol.% H₂O (when used), GHSV = 45,000 h⁻¹.

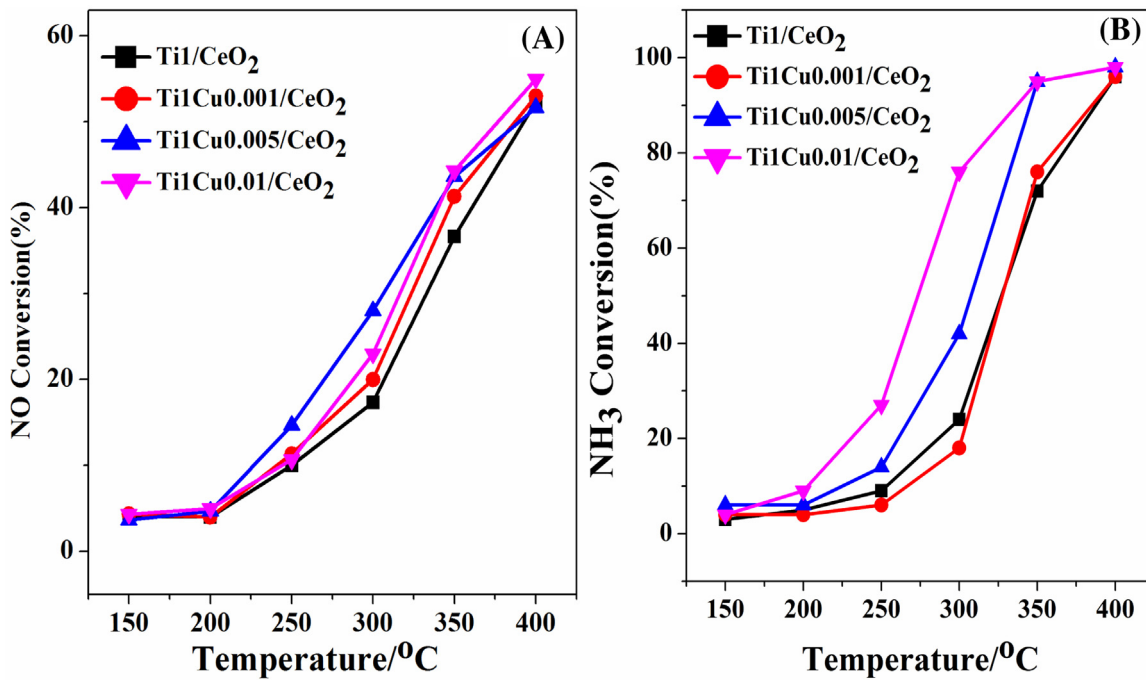


Fig. 3. (A) $\text{NO} + \text{O}_2$ (B) $\text{NH}_3 + \text{O}_2$ reaction over $\text{Ti1}/\text{CeO}_2$ and $\text{Ti1Cu}/\text{CeO}_2$ catalysts, Reaction conditions: 500 ppm NO/NH_3 , 5 vol.% O_2 .

3. Results and discussion

3.1. Catalytic test results

3.1.1. Effect of copper loading on catalytic performance

The NO conversion and N_2 selectivity as a function of temperature in the NH_3 -SCR reaction over $\text{Ti1Cu}/\text{CeO}_2$ catalysts were presented in Fig. 1(A) and (B). As well, $\text{Ti1}/\text{CeO}_2$ and $\text{V}_2\text{O}_5\text{-WO}_3/\text{TiO}_2$ catalysts are supplied as references. Results showed that the $\text{Ti1Cu}/\text{CeO}_2$ catalysts had relatively high NO conversion in the temperature range of 200–400 °C. Among them, $\text{Ti1Cu0.005}/\text{CeO}_2$ catalyst exhibited the best catalytic performance, of which the NO conversion can be maintained above 80% from 200 to 400 °C under a GHSV of 45000 h⁻¹. In addition, the NO conversion at 150 °C increased markedly from ca. 20% to ca. 60% comparing to $\text{Ti1}/\text{CeO}_2$, demonstrating even small amount of Cu loading could lead to the obvious change of the NH_3 -SCR performance. Interestingly, we found that the activities of $\text{Ti1Cu}/\text{CeO}_2$ catalysts exhibited a volcano-type tendency with the increase of Cu content. That is, the NO conversion of $\text{Ti1Cu}/\text{CeO}_2$ catalysts first increased as the Cu content elevated and then decreased as the Cu content increased further and the low-temperature activity was best when the molar ratio of Cu/Ce was 0.005. Compared with the traditional $\text{V}_2\text{O}_5\text{-WO}_3/\text{TiO}_2$ catalyst, we can also find that the $\text{Ti1Cu}/\text{CeO}_2$ catalysts exhibited distinct higher NO conversion in the low temperature range (150–250 °C). Regarding on the N_2 selectivity, it can be noticed from Fig. 1(B) that the N_2 selectivity values of $\text{Ti1}/\text{CeO}_2$, $\text{Ti1Cu0.001}/\text{CeO}_2$ and $\text{Ti1Cu0.005}/\text{CeO}_2$ catalysts were nearly 100% in the whole studied temperature range. However, the N_2 selectivity of $\text{Ti1Cu0.01}/\text{CeO}_2$ catalyst had a slightly decline above 300 °C, which was probably related to the occurrence of unselective catalytic oxidation of NH_3 . In summary, the $\text{Ti1Cu0.005}/\text{CeO}_2$ catalyst was an optimal NH_3 -SCR catalyst at low temperature with over 80% NO removal efficiency and 100% N_2 selectivity at 200–400 °C.

3.1.2. Effect of H_2O and SO_2

In practical working conditions, water vapor and SO_2 were participants in the flue gas and had a strong influence on NO con-

version. Thus, the $\text{SO}_2/\text{H}_2\text{O}$ durability of these catalysts was further investigated in the present work. The influence of individual SO_2 on each sample at 200 °C and 300 °C was tested as a function of time and the results were illustrated in Fig. 2(A) and Fig. 2(B) respectively. As shown in Fig. 2(A), the NO conversions over all samples at 200 °C declined continuously when 200 ppm SO_2 was injected into the feed gas. However, the results in Fig. 2(B) showed that when the temperature increased to 300 °C, the NO conversions of these catalysts could remain unchanged at least for 20 h, indicated the excellent SO_2 -tolerance ability at 300 °C. As the ceria was the dominant component in the $\text{Ti1}/\text{CeO}_2$ and $\text{Ti1Cu}/\text{CeO}_2$ catalysts, the SO_2 -resistance of pure CeO_2 was also tested as a comparison and the result was presented in Fig. 2(B). We can observe that the NO conversion of CeO_2 firstly increased from ca. 40% to ca. 85% because of the synergistic catalysis between surface sulfates and bulk CeO_2 [14,25] and then declined continuously. In addition, the experiments of $\text{H}_2\text{O}/\text{H}_2\text{O}+\text{SO}_2$ poisoning tests at 300 °C over $\text{Ti1}/\text{CeO}_2$ and $\text{Ti1Cu}/\text{CeO}_2$ were also carried out and the results were showed in Fig. 2(C). After 5 vol.% H_2O was introduced, the catalysts can still keep nearly initial NO conversion. Thus, adding 5 vol.% H_2O in the feed gas at 300 °C had nearly no influence on the catalytic performance of these catalysts. Afterwards, 200 ppm SO_2 were also injected into the catalytic reaction condition, the NO conversion started to decrease slowly and maintained ca. 60% after 12 h. And the NO removal efficiency could only recover to about 80% after SO_2 and H_2O were removed. So the deactivation effect in the coexistence of SO_2 and H_2O was irreversible and co-existing of H_2O and SO_2 had a more remarkable negative influence on the NO removal efficiency than individual SO_2 because of the competitive adsorption of NH_3 and H_2O [26–28].

3.1.3. $\text{NO}/\text{NH}_3 + \text{O}_2$ reaction on $\text{Ti1}/\text{CeO}_2$ and $\text{Ti1Cu}/\text{CeO}_2$

Many researchers have reported that the process of NO oxidation to NO_2 played an important role in promoting the low temperature activity of NH_3 -SCR catalysts by accelerating the “fast SCR” process: $\text{NO} + \text{NO}_2 + 2\text{NH}_3 \rightarrow 2\text{N}_2 + 3\text{H}_2\text{O}$ [29–32]. To explore this point, NO oxidation reaction was conducted and the result was displayed in Fig. 3(A). It can be seen that the NO conversions

Table 1

Textual and structural parameters of CeO_2 and the related catalysts of supports and catalysts.

Samples	S_{BET} ($\text{m}^2 \text{g}^{-1}$)	Average crystallite size (nm)	$I_a/(I_a + I_b)\%$	FWHM (cm^{-1})
CeO_2	61.2	9.8	—	—
Ti1/ CeO_2	59.1	17.5	4.35	26.7
Ti1Cu0.001/ CeO_2	58.4	14.6	6.12	26.8
Ti1Cu0.005/ CeO_2	57.0	15.7	8.60	28.1
Ti1Cu0.01/ CeO_2	55.5	15.3	10.27	29.6

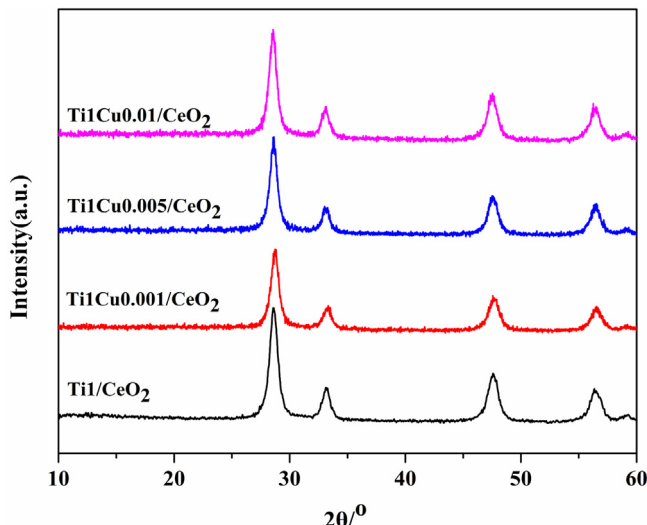


Fig. 4. XRD results of the $\text{Ti1}/\text{CeO}_2$ and $\text{Ti1Cu}/\text{CeO}_2$ catalysts.

of $\text{Ti1Cu}/\text{CeO}_2$ were all higher than that of $\text{Ti1}/\text{CeO}_2$ at identical temperature point. Therefore, we can reasonably deduced that the NH_3 -SCR reaction can more easily proceed via the “fast SCR” reaction route over $\text{Ti1Cu}/\text{CeO}_2$ catalysts, which was consistent with the SCR performance. On the other hand, the activation of NH_3 at low temperatures was also very important for improving low temperature activity. So the separate NH_3 oxidation experiments were executed. As shown in Fig. 3(B), after Cu doping, NH_3 oxidation activity of $\text{Ti1Cu}/\text{CeO}_2$ catalysts were greatly enhanced. The light-off temperature with 50% NH_3 conversion of $\text{Ti1Cu0.005}/\text{CeO}_2$ and $\text{Ti1Cu0.01}/\text{CeO}_2$ catalysts respectively shifted to ca. 270 °C and 305 °C comparing with $\text{Ti1}/\text{CeO}_2$. This was good for the activation of NH_3 or NH_4^+ adsorbed species on the $\text{Ti1Cu}/\text{CeO}_2$ catalyst surface [33,34]. However, a large body of research demonstrated that excessive NH_3 oxidation could lead to the decline of catalytic activity and N_2 selectivity at high temperature [35,36]. Therefore, the SCR performance was closely related to the loading content of copper of $\text{Ti1Cu}/\text{CeO}_2$ catalysts, which will be discussed by the following characterizations.

3.2. Structural properties (XRD, BET and Raman)

The XRD results of the obtained catalysts were displayed in Fig. 4. In the XRD patterns of $\text{Ti1}/\text{CeO}_2$ and $\text{Ti1Cu}/\text{CeO}_2$, all the samples only exhibited characteristic diffraction peaks assigned to CeO_2 which showed a cubic fluorite-type structure [PDFICDD34-0394]. The disappearance of TiO_2 and crystalline CuO diffraction peaks indicated that they were well-dispersed on the surface of CeO_2 support or their particle size was smaller than the detection limit of XRD. Table 1 summarized the BET specific areas of all the catalysts and the average crystallite which was calculated by the Scherrer equation based on the XRD result. From the above results, it was clearly seen that the introduction of Cu do not have pronounced influence on crystal structure over $\text{Ti1Cu}/\text{CeO}_2$ catalysts.

Table 2

The surface acid property and EPR signal of $\text{Ti1}/\text{CeO}_2$ and $\text{Ti1Cu}/\text{CeO}_2$ catalysts.

Samples	Total acids (a.u.)	$I_{\text{Bacids}}/I_{\text{Lacids}}\%$	The relative EPR signal intensity
$\text{Ti1}/\text{CeO}_2$	7860	16.2	—
$\text{Ti1Cu0.001}/\text{CeO}_2$	10248	22.1	1
$\text{Ti1Cu0.005}/\text{CeO}_2$	15330	34.9	2.4
$\text{Ti1Cu0.01}/\text{CeO}_2$	15826	19.9	2.8

Raman spectroscopy was employed to detect the surface information of the catalyst, as a potential complementary characterization of XRD and the corresponding results were exhibited in Fig. 5(A). The Raman spectroscopy showed that all the samples exhibited a strong band at 462 cm^{-1} attributed to the F_{2g} vibration mode of cubic fluorite-type structure. The Raman bands corresponding to CuO and TiO_2 were absent for all the catalysts, indicating that CuO and TiO_2 were in the forms of highly dispersed state or/and clustered state on the surface of CeO_2 supports, consistent with the results of XRD. Moreover, we can observe that the characteristic F_{2g} vibration mode of these $\text{Ti1Cu}/\text{CeO}_2$ catalysts was broadened and shifted to lower frequency compared with $\text{Ti1}/\text{CeO}_2$ (Table 1), suggesting the strong interaction between CuO and CeO_2 . This indicated that a thin film of Cu–O–Ce solid solution may form on the surface of ceria lattice [37,38]. Based on the references reported, the broad peak between 580 and 650 cm^{-1} usually represented surface oxygen vacancies, the concentration of which was determined by I_{600}/I_{460} and the results were displayed in Table 1 [39,40]. It can be observed that the concentration of surface oxygen vacancies of $\text{Ti1Cu}/\text{CeO}_2$ catalysts was higher than that of $\text{Ti1}/\text{CeO}_2$, this offered another piece of evidence of copper being embedded in the lattice of ceria. Previous studies indicated that surface oxygen vacancies could facilitate the NO oxidation, so the low temperature catalytic activity of Cu modified Ti/CeO_2 could be improved via the fast SCR reaction [41].

3.3. EPR spectra analysis

EPR (Electron Paramagnetic Resonance) was a sensitive technique to investigate the oxidation states, surfaces, bulk coordination of transition metal oxides. It was reported that different state of copper species played diverse activity on NO reduction and NH_3 oxidation [32]. Hence, the EPR technique was employed to explore the identity of copper species over these samples. As shown in Fig. 5(B), these spectra were characteristics of a d^9 -like species, which were assigned to Cu^{2+} ions [42–44]. Previous studies reported isolated Cu^{2+} gave rise to narrow intense EPR signals and the interacting Cu^{2+} generated less EPR signal because of the interaction with neighboring cupric ions, while well-crystallized CuO phases produced EPR silent species [45–47]. Moreover, the relative intensity of EPR signal of copper species obtained by double integration algorithm decreased along with the formation of CuO clusters or/and crystallized CuO [42,48,49]. The relative EPR signal intensity of copper species over $\text{Ti1Cu0.001}/\text{CeO}_2$ and $\text{Ti1Cu0.005}/\text{CeO}_2$, $\text{Ti1Cu0.01}/\text{CeO}_2$ catalysts were calculated to be 1, 2.4, and 2.8, respectively (Table 2). For $\text{Ti1Cu0.01}/\text{CeO}_2$ sample, the relative EPR

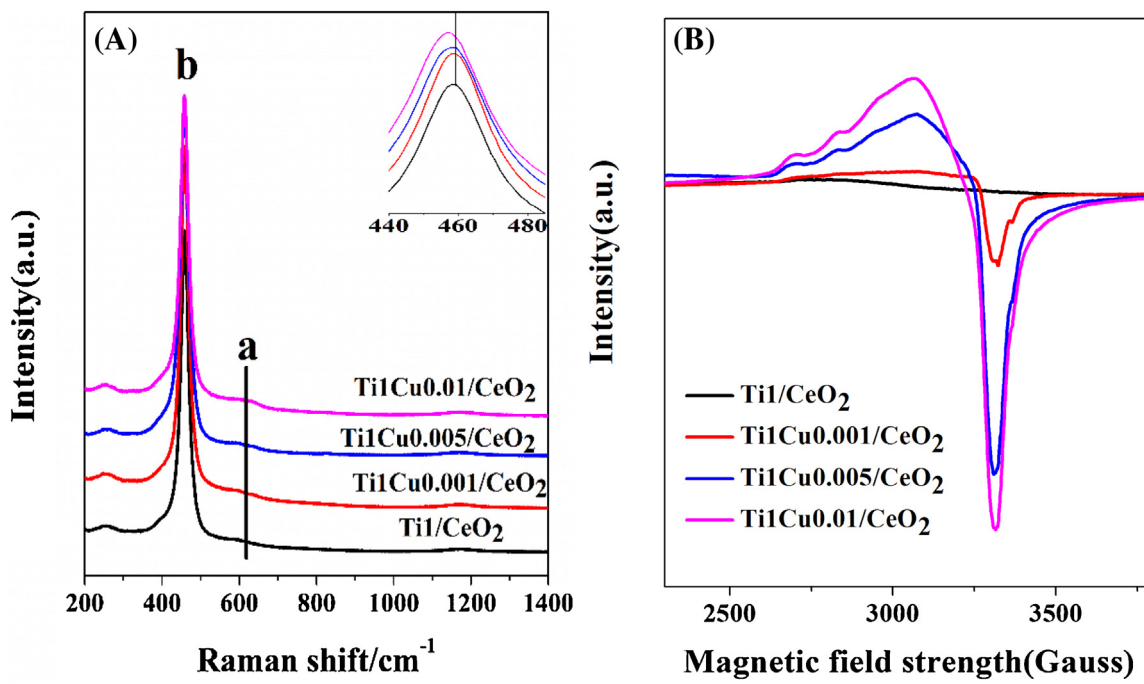


Fig. 5. (A) Raman (B) EPR results of the Ti1/CeO₂ and Ti1Cu/CeO₂ catalysts.

signal intensity was almost close to the Ti1Cu0.005/CeO₂, while its copper loading content was twice of Ti1Cu0.005/CeO₂. This phenomenon indicated the formation of more clustered or/and crystallized copper species on Ti1Cu0.01/CeO₂ surface. In other words, Ti1Cu/CeO₂ samples were inclined to form ‘CuO’ clusters species and crystallized CuO with the Cu loading increasing. Some researches suggested that the presence of excessive clustered CuO and crystallized CuO species may cause the occurrence of NH₃-SCR side reaction ($4\text{NH}_3 + 3\text{O}_2 \rightarrow 2\text{N}_2 + 6\text{H}_2\text{O}$) and had negative influence on NH₃-SCR performance [22]. Thus, the SCR performance of Ti1Cu0.01/CeO₂ catalyst began to decline due to the formation of more clustered CuO species compared to Ti1Cu0.005/CeO₂.

3.4. Reduction properties (H₂-TPR)

The redox property was a key factor for the catalytic activity of NH₃-SCR catalysts. Therefore, H₂-TPR experiment was employed to evaluate the reducibility of Ti1Cu/CeO₂ and Ti1/CeO₂ catalysts and the obtained results were illustrated in Fig. 6. In general, all samples exhibited three reduction peaks which were similar to the reduction behavior in other report [22]. The peak α was attributed to the reduction of surface active oxygen species, for Ti1Cu/CeO₂ catalysts the reduction of copper oxide species was included; the peak β and peak γ correspond to the reduction of subsurface layers or deeper interior of CeO₂ and bulk CeO₂ with the reduction of TiO₂, respectively. As shown in Fig. 6, the peak α of all Ti1Cu/CeO₂ catalysts showed lower onset reduction temperature comparing to Ti1/CeO₂. This implied that the surface active oxygen species were more active over Ti1Cu/CeO₂ samples, which was favourable to the oxidation of NO to NO₂, facilitating the low temperature activity via “fast SCR” reaction. Meanwhile, the peak β also shifted to lower reduction temperature over the Ti1Cu0.005/CeO₂ and Ti1Cu0.01/CeO₂ samples which indicated the surface CeO₂ became easily to be reduced. Therefore, the addition of Cu could promote the reduction of surface active oxygen species and surface CeO₂, which agreed well with the result as other works reported [16,50]. We also noticed that the shifts of the peak α and peak β over Ti1Cu0.01/CeO₂ catalyst were extremely significant (dif-

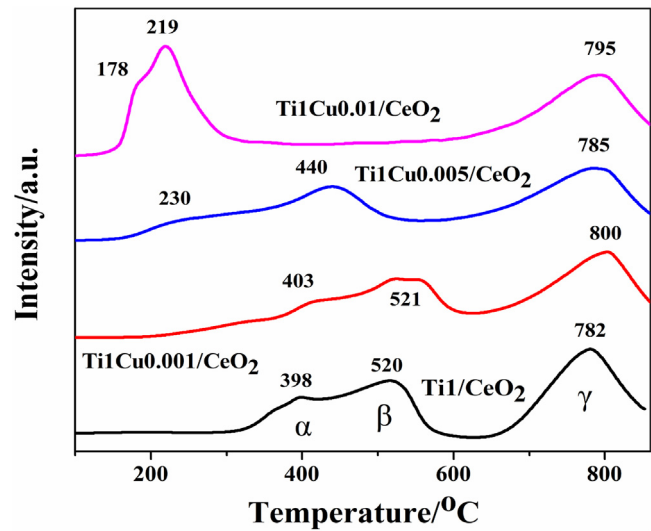


Fig. 6. H₂-TPR results of the Ti1/CeO₂ and Ti1Cu/CeO₂ catalysts.

ferred about 200 °C) as compared to Ti1/CeO₂. This was probably because of the formation of ‘CuO’ clusters species or/and crystallized CuO over Ti1Cu0.01/CeO₂ with the increasing of Cu loading as the EPR result had proved. So, it was reasonable to deduce that there was a strong interaction between Ce and Cu in these Ti1Cu/CeO₂ catalysts, which displayed a synergistic effect in the reducibility of the catalysts, leading to the enhancement of catalytic activity. However, for Ti1Cu0.01/CeO₂ catalyst, they didn't show the best catalytic performance. Some studies reported that the excessively strong redox ability could cause the unexpected NH₃ unselective oxidation, thus decrease the NO conversion and the N₂ selectivity [22,51,52]. Therefore, only the proper copper loading of the catalyst with optimal reduction properties exhibited the superior performances during the NH₃-SCR reaction.

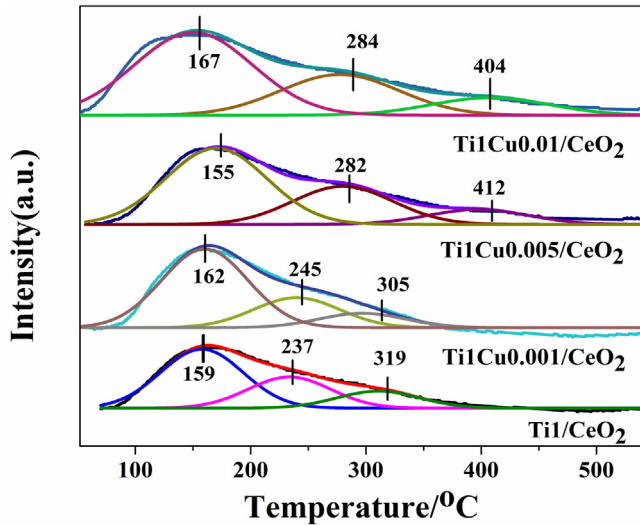


Fig. 7. NH₃-TPD results of the Ti1/CeO₂ and Ti1Cuy/CeO₂ catalysts.

3.5. Surface acidity properties (NH₃-TPD)

The surface acidity of the catalyst was of significant importance to the catalytic performance in NH₃-SCR reaction, besides the proper reducibility of the catalyst [53–55]. Temperature programmed desorption of ammonia (NH₃-TPD) experiments were carried out to investigate the amount and strength of surface acidity over these samples. The NH₃-TPD profiles of Ti1/CeO₂ and Ti1Cuy/CeO₂ catalysts all displayed a broad peak about from 100 to 500 °C, which were divided into three peaks as defined in Fig. 7. The peak around 160 °C was assigned to physical/weakly absorbed NH₃. The peaks between 200 °C and 500 °C could be ascribed to chemical/strong absorbed NH₃ [36,56]. The quantitative analysis results of NH₃-TPD were summarized in Table 2. We can find that the total acid amount of these catalysts followed the sequence of Ti1Cu0.01/CeO₂ > Ti1Cu0.005/CeO₂ > Ti1Cu0.001/CeO₂ ≈ Ti1/CeO₂, and both the amounts of weak and strong acid site increased respectively for the addition of copper. Moreover, the desorption temperature of strong adsorbed NH₃ over Ti1Cu0.005/CeO₂ and Ti1Cu0.01/CeO₂ catalysts moved to higher temperature, suggesting NH₃ adsorption on these samples was more stable. Thus, NH₃-TPD results indicated that loading Cu on Ti1/CeO₂ catalyst can markedly enhance its surface acid property.

3.6. Surface chemical states analysis (XPS)

To identify the effect of copper on the state of surface species, Ti1/CeO₂ and Ti1Cuy/CeO₂ catalysts ($y=0.001, 0.005, 0.01$) were measured by XPS. Fig. 8 illustrated the XPS spectra for Ce 3d and O 1s respectively, and the corresponding surface atomic concentrations and the relative concentration ratio of different oxidation states were summarized in Table 3. The XPS spectra of Ce 3d were fitted with eight peaks for each sample by Gaussian-Lorentz fitting in Fig. 8(A) [9,10]. The peaks denoted as u and v were attributed to the Ce 3d_{5/2} and Ce 3d_{3/2} spin-orbit components, respectively. According to the relevant researches [14,57], the bands labeled as u''' and v''', u'' and v'', u and v were assigned to Ce⁴⁺, while the bands of u' and v' were related to Ce³⁺. It was apparent to observe that the oxidation state of Ce over all the samples was mainly +4 and a part of Ce³⁺ co-exists on the surface of these cerium-containing catalysts. The content of Ce³⁺ can be estimated by calculating the area ratio of these binding energy bands by the following equation [28,35,36]: Ce³⁺(%) = Su' + Sv' / Σ(Su + Sv) × 100. As listed in Table 3, the relative concentration of Ce³⁺ increased with the introduction

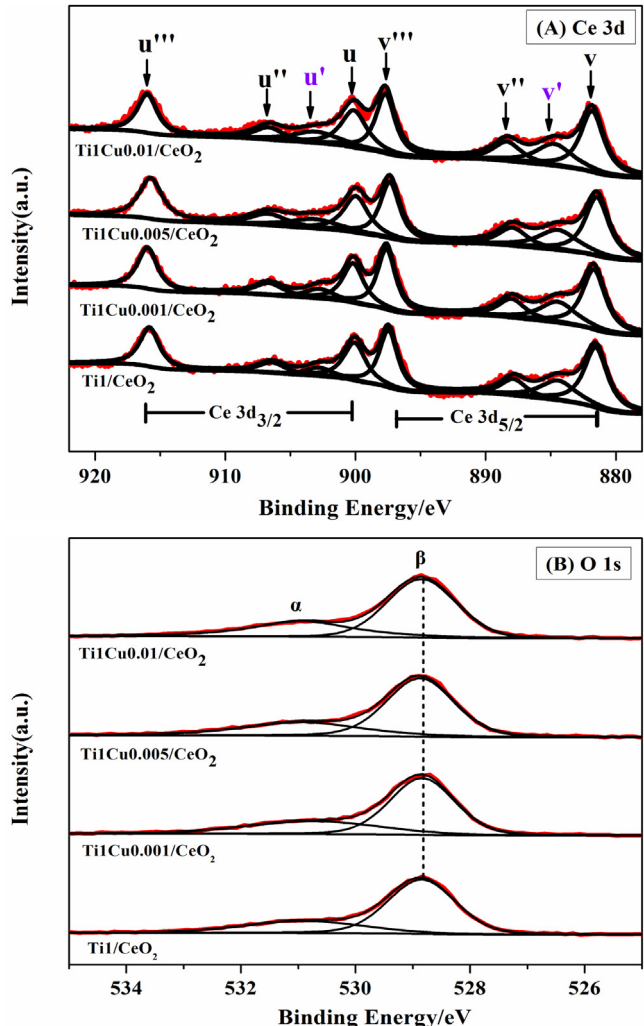
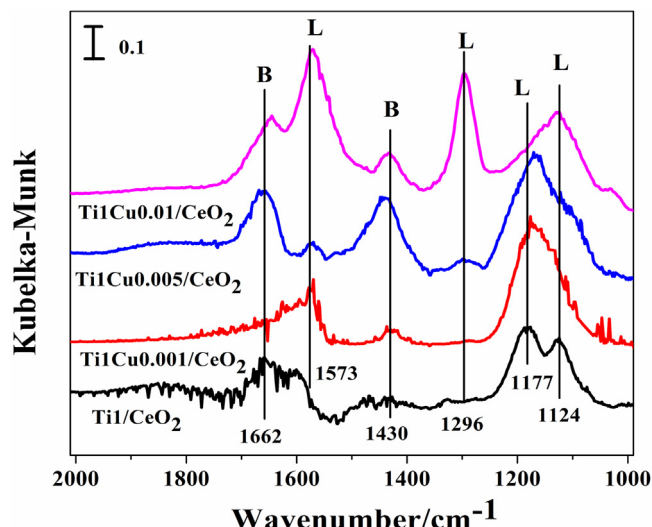


Fig. 8. XPS results of the Ti1/CeO₂ and Ti1Cuy/CeO₂ catalysts: (A) Ce 3d (B) O 1s.

of Cu. This demonstrated that the introduction of Cu resulted in great conversion of Ce⁴⁺ to Ce³⁺ on the catalyst surface compared to that on pure titanium oxide supported on CeO₂. The generation of Ce³⁺ may be due to the formation of the thin film of Cu—O—Ce solid solution on the surface. In addition, the O 1s XPS information of these samples was presented in Fig. 8 (B). The peak at 531.2 eV was considered as surface adsorbed oxygen species (denoted as O_α), and the band of O_β at 529.8 eV was ascribed to lattice oxygen species [9,58]. The O_α/(O_α+O_β) ratio of all the samples were calculated by the area integral of O_α and O_β. It could be found that the relative concentration ratio of O_α over Ti1Cuy/CeO₂ catalysts was higher than that of Ti1/CeO₂ (Table 3), suggesting that the surface oxygen species were greatly increased after the introduction of copper. The above XPS results indicated that the addition of minor content of copper to Ti1/CeO₂ could increase the ratio of the Ce³⁺/Ce. And the generation of Ce³⁺ could create a charge imbalance and vacancies on the catalysts surface [58], leading to the increase of surface oxide defects or hydroxyl-like groups. In the NH₃-SCR reaction, the surface adsorbed oxygen species was more active than the lattice oxygen species due to its higher mobility [31]. This meant that the Cu modified Ti1/CeO₂ catalyst might have better activity for the NO oxidation to NO₂ than the Ti1/CeO₂ catalyst, thus promoting the occurrence of “fast-SCR” reaction and enhance the NO removal efficiency at low temperature. The NH₃ adsorption capacity was also enhanced due to the production of a larger amount of surface hydroxyl groups. The enhancement of

Table 3The fitting data of XPS over Ti1/CeO₂ and Ti1Cu_y/CeO₂.

Samples	Atomic concentration/mol.%				Atomic ratio/%	
	Ce	Ti	O	Cu	Ce ³⁺ /(Ce ³⁺ + Ce ⁴⁺)	O _α /(O _α + O _β)
Ti1/CeO ₂	13.81	5.39	52.59	–	17.4	29.93
Ti1Cu0.001/CeO ₂	10.68	10.62	53.72	–	18.7	31.27
Ti1Cu0.005/CeO ₂	11.03	10.18	54.96	–	19.8	32.52
Ti1Cu0.01/CeO ₂	14.51	5.70	52.72	0.67	21.7	34.81

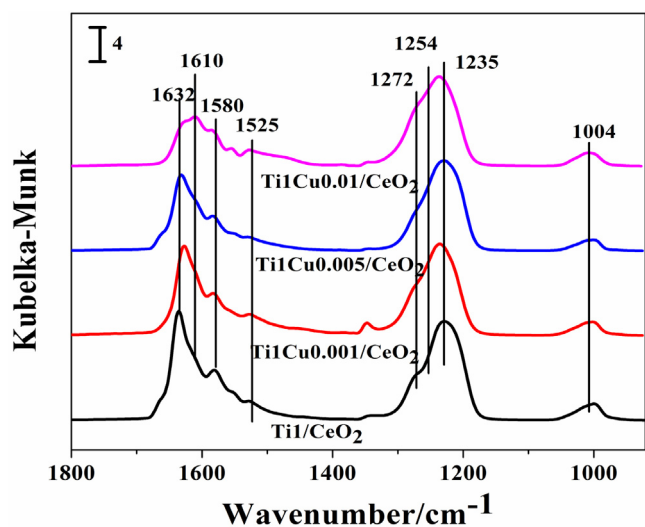
**Fig. 9.** NH₃ absorption *in situ* DRIFTS of the Ti1/CeO₂ and Ti1Cu_y/CeO₂ catalysts at room temperature.

NH₃ adsorption behavior over the Cu modified Ti1/CeO₂ catalyst would be discussed later.

3.7. In situ DRIFT analysis

3.7.1. NH₃/NO + O₂ adsorption

In the NH₃-SCR reaction, especially in the low-temperature range, both NH₃ and NO_x can adsorb on the catalyst surface and participate in the NO_x reduction process. Therefore, *in situ* DRIFTS spectra of NH₃/NO_x adsorption over Ti1/CeO₂ and Ti1Cu_y/CeO₂ catalysts at 50 °C were recorded in Fig. 9. When NH₃-N₂ (1% of NH₃ by volume) was introduced into the DRIFTS cell for 1 h and then purged by high purified N₂ for 20 min, several vibration bands were detected on all catalysts surface in the range of 1000–1800 cm⁻¹. On the basis of the literatures [14,15], the bands at about 1420–1450 cm⁻¹ and 1650–1690 cm⁻¹ were ascribed to the asymmetric bending vibration of N-H bond in NH⁴⁺ chemisorbed on Brønsted acid sites [39,59], while the bands at 1090–1290 cm⁻¹ and 1590–1610 cm⁻¹ were assigned to the asymmetric and symmetric bending vibrations of N-H bond in NH₃ coordinated with Lewis acid sites. The obtained results indicated that there were both Lewis and Brønsted acid sites on the surface of all samples. For Ti1Cu_y/CeO₂ samples, after introduction of Cu, the bands attributed to Lewis and Brønsted acid sites were much stronger than that of Ti1/CeO₂, which was consistent with the NH₃-TPD results. Herein, the more Brønsted acid sites generated on the Ti1Cu_y/CeO₂ catalysts surface were resulted from the Ce³⁺ species by Cu modification. Lei [15] thought that the coordinated NH₃ can also be absorbed on CuO, which brought about a small amount of Lewis acid sites. Thus, the L acid sites at 1296 cm⁻¹ were caused by the presence of the CuO on the surface of support. The ratio of the area of Brønsted and Lewis acid sites was shown in Table 2 and the relative amount of Brønsted acid sites of Ti1Cu0.005/CeO₂ was

**Fig. 10.** NO + O₂ absorption *in situ* DRIFTS of the Ti1/CeO₂ and Ti1Cu_y/CeO₂ catalysts at room temperature.

highest in all the samples. Since the Brønsted acid site was helpful for the SCR activity at low temperatures, Ti1Cu_y/CeO₂ had the better low temperature catalytic performance than that of Ti1/CeO₂. On the basis of the above results, it indicated that the adsorption behavior of NH₃ was modified by the interaction between CuO and supports.

The NO + O₂ adsorption of the catalysts was also investigated by *in situ* DRIFT and the obtained spectra were showed in Fig. 10. For Ti1/CeO₂ and Ti1Cu_y/CeO₂ catalysts, when NO + O₂ mixed gases were introduced into the DRIFTS cell at 50 °C, several vibration bands can be observed in the range of 1000–1800 cm⁻¹: bridging bidentate nitrates (1632 cm⁻¹); bridging monodentate nitrates (1610 and 1235 cm⁻¹); bidentate nitrates (1020, 1580 and 1254 cm⁻¹) and monodentate nitrates (1525 and 1272 cm⁻¹) [15,60]. After the introduction of CuO, the types of surface adsorbed nitrate species of Ti1Cu_y/CeO₂ samples were unchanged, but the adsorption intensity became weaker, especially the bands for bridging nitrates (1632 and 1610 cm⁻¹). Thus, it was deduced that the appearance of CuO weakened the adsorption ability of bridging nitrate species over the Ti1Cu_y/CeO₂ catalysts. Meanwhile, the NO + O₂ adsorption-desorption experiments from 50 to 375 °C were also played to investigate the adsorption differences of nitrogen oxides between these samples (in Figs. S1–4). The intensity of all peaks uniformly decreased with the rise in temperature and the intensity of these nitrogen oxides on the surface of Ti1/CeO₂ were stronger than those of Ti1Cu_y/CeO₂ at the same temperature, which was more obvious for the bridging nitrate. This means that the adsorbed nitrate species on Ti1Cu_y/CeO₂ catalysts were weaker than that Ti1/CeO₂, indicating that the adsorbed nitrate species were more easily decomposed to gas phase than Ti1/CeO₂. Our previous study had found that the competition adsorption happened between bridging nitrates and gas NH₃ [60]. Therefore, it can be proposed that adding CuO resulted in weakening the adsorption

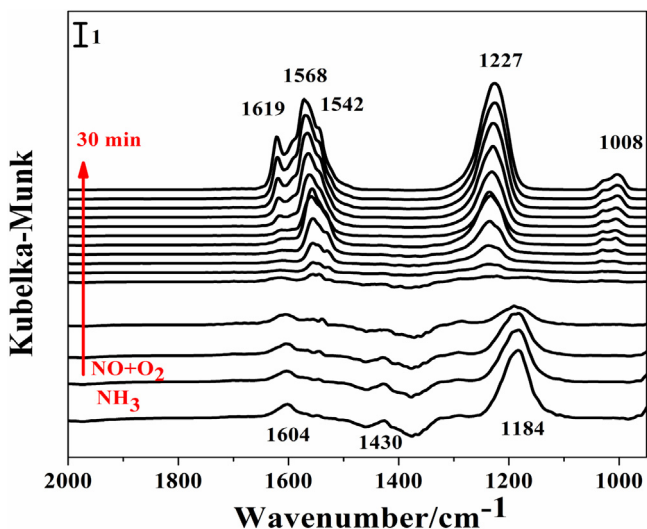


Fig. 11. $\text{NO} + \text{O}_2$ absorption *in situ* DRIFTS of TiCu0.005/CeO_2 pre-absorbed NH_3 at 200°C .

ability of nitrate species over $\text{Ti1Cu}/\text{CeO}_2$, leading to more active sites for NH_3 adsorption, which were responsible for the improvement of NO_x catalytic conversion.

3.7.2. In situ DRIFTS of the reaction between (a) $\text{NO} + \text{O}_2$ and adsorbed NH_3 species, (b) NH_3 and adsorbed $\text{NO} + \text{O}_2$ species over Ti1Cu0.005/CeO_2 catalyst

To clarify the reaction pathways of adsorbed NH_3 species and NO on Ti1Cu0.005/CeO_2 catalyst, the interaction between $\text{NO} + \text{O}_2$ and pre-adsorbed NH_3 as a function of time was employed. NH_3 was pre-adsorbed for 60 min followed by high purified N_2 purged at 200°C , then $\text{NO} + \text{O}_2$ was injected. As shown in Fig. 11, the coordinated NH_3 absorbed on Lewis (1184 and 1604 cm^{-1}) and Brønsted acid sites (1430 cm^{-1}) were formed on the surface of Ti1Cu0.005/CeO_2 catalyst. When the $\text{NO} + \text{O}_2$ was introduced, the bands attribute to adsorbed NH_3 species (both on L and B acid sites) diminished rapidly accompanying the generation of nitrate species (1008 , 1227 , 1568 cm^{-1} for bidentate nitrates, 1542 cm^{-1} for monodentate nitrates, 1619 cm^{-1} for bridging nitrates). The phenomenon indicated that E-R reaction pathways proceeded via pre-adsorbed NH_3 and the NO_x gas over Ti1Cu0.005/CeO_2 sample [59]. Moreover, the coordinated NH_3 on B acid sites disappeared faster than that on L acid sites, indicating NH_3 coordinated with B acid sites was more active in NH_3 -SCR reaction. The similar result was observed on $\text{Ti1}/\text{CeO}_2$ (in Fig.S5). Compared the results with $\text{Ti1}/\text{CeO}_2$ and Ti1Cu0.005/CeO_2 , we found that the NH_3 adsorbed on Ti1Cu0.005/CeO_2 disappeared faster than that on $\text{Ti1}/\text{CeO}_2$, which suggested that the NH_3 species adsorbed on Ti1Cu0.005/CeO_2 could take part in the NH_3 -SCR reaction easily by addition of Cu. Meanwhile, the $\text{NO} + \text{O}_2$ adsorption DRIFTS experiment showed that the nitrate species were more easily formed on the surface of the $\text{Ti1}/\text{CeO}_2$ sample, which could occupy more active sites that were for NH_3 adsorption. This means that the Ti1Cu0.005/CeO_2 could release more active sites for NH_3 adsorption by comparison with the $\text{Ti1}/\text{CeO}_2$ sample. Based on the above results, it can be proposed that doping Cu resulted in promoted activation of NH_3 , and thus further improved the performance of the NH_3 -SCR reaction.

In addition, we carried out the reaction between NH_3 and pre-adsorbed $\text{NO} + \text{O}_2$ at 200°C with the time, and the corresponding results were exhibited in Fig. 12. For Ti1Cu0.005/CeO_2 sample, bridging nitrates at 1624 , 1593 and 1230 cm^{-1} , bidentate nitrates at 1559 cm^{-1} and monodentate nitrates at 1543 cm^{-1} were formed on the catalyst surface when $\text{NO} + \text{O}_2$ was introduced into DRIFT cell.

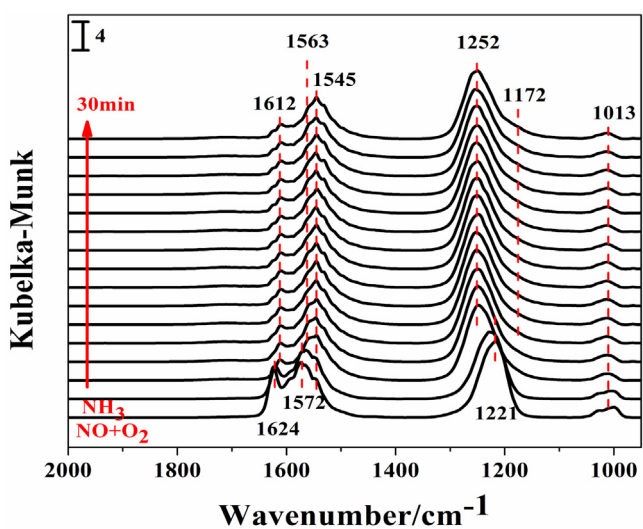


Fig. 12. NH_3 absorption *in situ* DRIFTS of TiCu0.005/CeO_2 pre-absorbed $\text{NO} + \text{O}_2$ at 200°C .

Then NH_3 passed over the Ti1Cu0.005/CeO_2 catalyst, the band at 1624 and 1593 cm^{-1} attributed to bridging nitrates vanished, and the band ascribed to the deformation nitrate species shifted from 1230 to 1252 cm^{-1} [61]. And the bands assigned to coordinated NH_3 on Lewis acid sites (1172 , 1612 cm^{-1}) appeared on catalyst surface accompanying the disappearance of bridging nitrates. This was because NH_3 molecular could snatch an adsorption site from bridging nitrates to form one L acid, and then bridging nitrates transform to monodentate and chelating bidentate nitrates [60]. Moreover, the intensities of both nitrate species and NH_3 bounded to L acids (1175 , 1609 cm^{-1}) remained unchanged after injecting NH_3 for 30 min, indicating the adsorbed nitrate species could not react with the adsorbed NH_3 species, which suggested that NH_3 -SCR reaction didn't proceed through Langmuir-Hinshelwood (L-H) mechanism. The above results indicated that the NH_3 and bridging nitrates could adsorb on the same active sites. Combined with the $\text{NO} + \text{O}_2$ DRIFTS results, the adding of copper over $\text{Ti1}/\text{CeO}_2$ catalyst weaken the adsorption of bridging nitrate species, and thus improve the adsorption capacity of NH_3 and promoted NH_3 -SCR reaction to proceed smoothly by Eley-Rideal (E-R) mechanism.

4. Conclusion

In this work, minor copper modified $\text{Ti1}/\text{CeO}_2$ catalysts were prepared and used for low temperature selective reduction of NO by NH_3 . The activity results demonstrated that these catalysts followed the order of $\text{Ti1Cu0.005/CeO}_2 > \text{Ti1Cu0.01/CeO}_2 > \text{Ti1Cu0.001/CeO}_2 > \text{Ti1}/\text{CeO}_2$. As well, outstanding resistance to sulfur dioxide was obtained. With the help of Raman, XPS, NH_3 -TPD and *in situ* DRIFT characterizations, it was shown that $\text{Ti1Cu}/\text{CeO}_2$ catalysts got higher concentration of Ce^{3+} species and surface active O_α , more surface acid sites and weaker adsorption ability of bridging nitrate species than $\text{Ti1}/\text{CeO}_2$, which were supposed to be important for NO conversion. Besides, moderate reducibility and the highest relative amount of Brønsted acid sites of Ti1Cu0.005/CeO_2 helped it obtain the best catalytic performance among $\text{Ti1Cu}/\text{CeO}_2$ catalysts. Mechanism investigation via *in situ* DRIFT spectroscopy suggested that the reaction mainly proceed by Eley-Rideal mechanism over these catalysts. Moreover, EPR results proved that there were likely to be different types of Cu containing species present over $\text{Ti1Cu}/\text{CeO}_2$ catalysts, depending on the Cu loading amount. Combined with active results, we proposed that the CuO clusters

(high CuO loading) formed on catalysts surface were more effective for NH₃ oxidation to NO_x than the isolated Cu species (low CuO loading), limiting the availability of NH₃ for NO reduction and thus decreased NO conversion and N₂ selectivity. Therefore, the NH₃-SCR performance of Ti1Cu_y/CeO₂ catalysts was much affected by the change of very small amounts of copper content, which can be used as a guideline for tuning the NH₃-SCR performance of ceria-based or other catalysts.

Acknowledgements

This work was supported by National High-tech Research and Development (863) Program of China (2015AA03A401), Science and Technology Support Program of Jiangsu Province (Industrial, BE2014130), Scientific Research Project of Environmental Protection Department of Jiangsu Province (2016048), National Natural Science Foundation of China (21303082, 21573105, 21670182, 21503115, 21607019) and the Doctoral Fund of Ministry of Education of China (2013009111005).

Appendix A. Supplementary data

Supplementary data associated with this article can be found, in the online version, at <http://dx.doi.org/10.1016/j.apcatb.2017.02.041>.

References

- [1] M. Kang, E.D. Park, J.M. Kim, J.E. Yie, *Appl. Catal. A: Gen.* 327 (2007) 261–269.
- [2] S. Andreoli, F.A. Deorsola, R. Pirone, *Catal. Today* 253 (2015) 199–206.
- [3] S. Ding, F. Liu, X. Shi, K. Liu, Z. Lian, L. Xie, H. He, *ACS Appl. Mater. Interfaces* 7 (2015) 9497–9506.
- [4] X. Du, X. Gao, Y. Fu, F. Gao, Z. Luo, K. Cen, *J. Colloid Interface Sci.* 368 (2012) 406–412.
- [5] S.S.R. Putluru, L. Schill, A. Godiksen, R. Poreddy, S. Mossin, A.D. Jensen, R. Fehrmann, *Appl. Catal. B: Environ.* 183 (2016) 282–290.
- [6] B. Shen, Y. Wang, F. Wang, T. Liu, *Chem. Eng. J.* 236 (2014) 171–180.
- [7] R. Gao, D. Zhang, X. Liu, L. Shi, P. Maitarad, H. Li, J. Zhang, W. Cao, *Catal. Sci. Technol.* 3 (2013) 191–199.
- [8] L. Lietti, I. Nova, G. Ramis, L. Dall'Acqua, G. Busca, E. Giamello, P. Forzatti, F. Bregani, *J. Catal.* 187 (1999) 419–435.
- [9] W. Shan, F. Liu, H. He, X. Shi, C. Zhang, *Appl. Catal. B: Environ.* 115–116 (2012) 100–106.
- [10] T. Zhang, R. Qu, W. Su, J. Li, *Appl. Catal. B: Environ.* 176–177 (2015) 338–346.
- [11] Y. Zhang, Z. Xu, X. Wang, X. Lu, Y. Zheng, *Nano* 10 (2015) 1550050.
- [12] P. Li, Y. Xin, Q. Li, Z. Wang, Z. Zhang, L. Zheng, *Environ. Sci. Technol.* 46 (2012) 9600–9605.
- [13] X. Gao, Y. Jiang, Y. Fu, Y. Zhong, Z. Luo, K. Cen, *Catal. Commun.* 11 (2010) 465–469.
- [14] L. Zhang, L. Li, Y. Cao, X. Yao, C. Ge, F. Gao, Y. Deng, C. Tang, L. Dong, *Appl. Catal. B: Environ.* 165 (2015) 589–598.
- [15] L. Chen, Z. Si, X. Wu, D. Weng, *ACS Appl. Mater. Interfaces* 6 (2014) 8134–8145.
- [16] X.-S. Du, X. Gao, L.-W. Cui, Y.-C. Fu, Z.-Y. Luo, K.-F. Cen, *Fuel* 92 (2012) 49–55.
- [17] S.M. Lee, K.H. Park, S.C. Hong, *Chem. Eng. J.* 195–196 (2012) 323–331.
- [18] X. Li, J. Li, Y. Peng, H. Chang, T. Zhang, S. Zhao, W. Si, J. Hao, *Appl. Catal. B: Environ.* 184 (2016) 246–257.
- [19] Z. Liu, Y. Yi, J. Li, S.I. Woo, B. Wang, X. Cao, Z. Li, *Chem. Commun. (Camb.)* 49 (2013) 7726–7728.
- [20] M. Sakai, Y. Nagai, Y. Aoki, N. Takahashi, *Appl. Catal. A: Gen.* 510 (2016) 57–63.
- [21] Z. Qu, Z. Wang, X. Zhang, H. Wang, *Catal. Sci. Technol.* (2016).
- [22] J.H. Kwak, R. Tomkyn, D. Tran, D. Mei, S.J. Cho, L. Kovarik, J.H. Lee, C.H.F. Peden, J. Szanyi, *ACS Catal.* 2 (2012) 1432–1440.
- [23] L. Chen, J. Li, M. Ge, *Chem. Eng. J.* 170 (2011) 531–537.
- [24] S. Zhang, H. Li, Q. Zhong, *Appl. Catal. A: Gen.* 435–436 (2012) 156–162.
- [25] L. Zhang, W. Zou, K. Ma, Y. Cao, Y. Xiong, S. Wu, C. Tang, F. Gao, L. Dong, *J. Phys. Chem. C* 119 (2015) 1155–1163.
- [26] B. Shen, X. Zhang, H. Ma, Y. Yao, T. Liu, *J. Environ. Sci.* 25 (2013) 791–800.
- [27] R. Gao, D. Zhang, P. Maitarad, L. Shi, T. Rungratmongkol, H. Li, J. Zhang, W. Cao, *J. Phys. Chem. C* 117 (2013) 10502–10511.
- [28] H. Chang, J. Li, X. Chen, L. Ma, S. Yang, J.W. Schwank, J. Hao, *Catal. Commun.* 27 (2012) 54–57.
- [29] A. Grossale, I. Nova, E. Tronconi, D. Chatterjee, M. Weibel, *J. Catal.* 256 (2008) 312–322.
- [30] A. Grossale, I. Nova, E. Tronconi, *J. Catal.* 265 (2009) 141–147.
- [31] S. Yang, C. Wang, J. Li, N. Yan, L. Ma, H. Chang, *Appl. Catal. B: Environ.* 110 (2011) 71–80.
- [32] J. Chen, M. Shen, X. Wang, G. Qi, J. Wang, W. Li, *Appl. Catal. B: Environ.* 134–135 (2013) 251–257.
- [33] X. Yang, B. Zhao, Y. Zhuo, Y. Gao, C. Chen, X. Xu, *Environ. Sci. Technol.* 45 (2011).
- [34] C. Tang, H. Zhang, L. Dong, *Catal. Sci. Technol.* 6 (2016) 1248–1264.
- [35] X. Yao, L. Zhang, L. Li, L. Liu, Y. Cao, X. Dong, F. Gao, Y. Deng, C. Tang, Z. Chen, L. Dong, Y. Chen, *Appl. Catal. B: Environ.* 150–151 (2014) 315–329.
- [36] Y. Xiong, C. Tang, X. Yao, L. Zhang, L. Li, X. Wang, Y. Deng, F. Gao, L. Dong, *Appl. Catal. A: Gen.* 495 (2015) 206–216.
- [37] A.-P. Jia, G.-S. Hu, L. Meng, Y.-L. Xie, J.-Q. Lu, M.-F. Luo, *J. Catal.* 289 (2012) 199–209.
- [38] E.M. Slavinskaya, R.V. Gulyaev, A.V. Zadesenets, O.A. Stonkus, V.I. Zaikovskii, Y.V. Shubin, S.V. Korenev, A.I. Boronin, *Appl. Catal. B: Environ.* 166–167 (2015) 91–103.
- [39] X. Yao, Q. Yu, Z. Ji, Y. Lv, Y. Cao, C. Tang, F. Gao, L. Dong, Y. Chen, *Appl. Catal. B: Environ.* 130–131 (2013) 293–304.
- [40] X. Li, X.-Y. Quek, D.A.J. Michel Ligthart, M. Guo, Y. Zhang, C. Li, Q. Yang, E.J.M. Hensen, *Appl. Catal. B: Environ.* 123–124 (2012) 424–432.
- [41] C. Ciardelli, I. Nova, E. Tronconi, D. Chatterjee, B. Bandl-Konrad, *Chem. Commun. (Camb.)* (2004) 2718–2719.
- [42] J. Chen, Y. Zhan, J. Zhu, C. Chen, X. Lin, Q. Zheng, *Appl. Catal. A: Gen.* 377 (2010) 121–127.
- [43] H. Zhu, M. Shen, Y. Kong, J. Hong, Y. Hu, T. Liu, L. Dong, Y. Chen, C. Jian, Z. Liu, *J. Mol. Catal. A: Chem.* 219 (2004) 155–164.
- [44] P.W. Park, J.S. Ledford, *Appl. Catal. B: Environ.* 15 (1998) 221–231.
- [45] F. Mehran, S.E. Barnes, G.V. Chandrashekhar, T.R. McGuire, M.W. Shafer, *Solid State Commun.* 67 (1988) 1187–1189.
- [46] K.R.P. Parthasarathi Bera, P.R. Sarode, M.S. Hegde, S. Emura, R. Kumashiro, N.P. Lalla, *Chem. Mater.* 14 (2017) 3591–3601.
- [47] F. Wang, R. Büchel, A. Savitsky, M. Zalibera, D. Widmann, S.E. Pratsinis, W. Lubitz, F. Schüth, *ACS Catal.* 6 (2016) 3520–3530.
- [48] S. Hočevá, U.O. Krašovec, B. Orel, A.S. Aricó, H. Kim, *Appl. Catal. B: Environ.* 28 (2000) 113–125.
- [49] W. Liu, M. Flytzanistefanopoulos, *J. Catal.* 153 (1995) 304–316.
- [50] X. Gao, X.-S. Du, L.-W. Cui, Y.-C. Fu, Z.-Y. Luo, K.-F. Cen, *Catal. Commun.* 12 (2010) 255–258.
- [51] W. Miśta, M.A. Małecka, L. Kępiński, *Appl. Catal. A: Gen.* 368 (2009) 71–78.
- [52] M. Sun, G. Zou, S. Xu, X. Wang, *Mater. Chem. Phys.* 134 (2012) 912–920.
- [53] H.L. Koh, S.H. Lee, K.L. Kim, *React. Kinet. Catal. Lett.* 71 (2016) 239–244.
- [54] D.W. Kwon, K.B. Nam, S.C. Hong, *Appl. Catal. A: Gen.* 497 (2015) 160–166.
- [55] Z. Liu, H. Su, J. Li, Y. Li, *Catal. Commun.* 65 (2015) 51–54.
- [56] X. Zhao, L. Huang, H. Li, H. Hu, X. Hu, L. Shi, D. Zhang, *Appl. Catal. B: Environ.* 183 (2016) 269–281.
- [57] X. Yao, F. Gao, Q. Yu, L. Qi, C. Tang, L. Dong, Y. Chen, *Catal. Sci. Technol.* 3 (2013) 1355.
- [58] X. Gao, Y. Jiang, Y. Zhong, Z. Luo, K. Cen, *J. Hazard. Mater.* 174 (2010) 734–739.
- [59] T. Gu, R. Jin, Y. Liu, H. Liu, X. Weng, Z. Wu, *Appl. Catal. B: Environ.* 129 (2013) 30–38.
- [60] L. Zhang, L. Li, Y. Cao, Y. Xiong, S. Wu, J. Sun, C. Tang, F. Gao, L. Dong, *Catal. Sci. Technol.* 5 (2015) 2188–2196.
- [61] B. Guan, H. Lin, L. Zhu, Z. Huang, *J. Phys. Chem. C* 115 (2011) 12850–12863.